Int. J. Heat Mass Transfer. Vol. 29, No. 1, pp. 21–33, 1986
Printed in Great Britain

0017–9310/86 $3.00 + 0.00

Effects of electromagnetic stirring during the controlled solidification of tin

CHARLES VIVES and CHRISTIAN PERRY
Université d'Avignon, Laboratoire de Magnétohydrodynamique,
33 rue Louis Pasteur, 84000 Avignon, France

(*Received* 30 *April* 1985 *and in final form* 3 *July* 1985)

Abstract—The role of natural and forced convections during solidification of pure tin in an annular crucible was studied. The forced convection was generated by electromagnetic stirring. Maps of electromagnetic body forces and velocity fields were obtained for various stirring intensities and various positions of the solidification front. Temperature measurements made it possible to follow the evolution of the solidification front with time. These experiments were carried out from various degrees of superheat both in the absence and presence of electromagnetic stirring. A discussion is presented relating the metallurgical findings (macrostructure) to the heat and fluid flow measurements.

1. INTRODUCTION

IT IS AN established fact that in alloy solidification, convection in the vicinity of the solidification front may play a major role in affecting nucleation, the dendrite structure, segregation and the like which, in turn, determine the mechanical properties of the finished product. Thus stirring of the melt in continuous casting or in ingot solidification has frequently been found to provide a beneficial effect [1–3].

The greater part of the studies bearing on the role of heat transfer in solidification of metals and alloys have involved free convection. Szekely and Chhabra [4] have reported on the effect of natural convection on the shape and movement of the solidification front during the controlled solidification of lead. Theoretical and experimental work was also performed by Hills *et al.* with lead and lead–tin eutectic alloy [5] and, recently, by Gau and Viskanta, with a Lipowitz eutectic [6].

However, the liquid metal flows which affect convective heat transfer remain not well known. In fact, the measurement techniques of classical fluid mechanics are ineffectual because molten metals are opaque and, generally, have a high melting point. Nevertheless, a measurement method using a newly developed magnetic probe [7–9] now allows the determination of the local instantaneous values of the velocity vector, up to about 700°C.

The central purpose of this work is to compare in detail the effects of the natural convection and of the forced convection (created by an induction magnetic field) during the thermally controlled solidification of a pure metal contained in a mould. In this regard the application of a time-varying magnetic field is of particular interest because forced convection is readily generated in an easily controllable manner while avoiding direct contact between the stirrer and the melt. Electromagnetic stirring has been studied inside coreless induction furnaces [10–15], i.e. in the presence of the liquid phase exclusively, and other workers have reported on the effects of a travelling magnetic field on the solidification of alloys, particularly in the case of the continuous casting [1, 3].

The experimental device described in this work consisted of an annular crucible made of stainless steel, holding molten tin with a free surface. The inner cylinder was water cooled, while the outer cylinder was resistance heated. This arrangement allowed the controlled solidification of the melt. In addition the tin pool could be inductively stirred, using a cylindrical coil, supplied with a 50-Hz alternating current.

2. THE APPARATUS

The principal features of the apparatus are schematically presented in Fig. 1. The mould was made of stainless steel and consisted of an inner cylinder of 24-mm O.D., having a wall thickness of 2 mm, and of an outer cylinder with 174- and 170-mm I.D. respectively at the top and the bottom (in order to obtain an easy mould stripping); the O.D. was 179 mm. The bottom wall constituted a disk 8-mm thick, except for a crown 16-mm thick and 125 and 183 mm interior and exterior radii. The crucible contained 2 dm^3 of commercially pure tin.

The hot wall was heated by a resistance made up of seven turns of 8-mm diam. and traversed by an electric current (50 Hz). The caloric power was modulated at will, from 0 to 2200 W, by means of an autotransformer. The hot wall and the bottom of the furnace was thermally insulated by ceramic fibre (Triton Kaowool) 25-mm thick and the upper part of the annular container was covered by a rigid insulator (Siporex), 5-cm thick and 23-cm diam.

The inner wall was internally cooled by water at 20°C, with a flow rate of 1000 $dm^3\ h^{-1}$, allowing complete solidification of the metal in about 10 min. This flow rate was sufficient for the temperature of the water to remain practically unchanged (within 1°C) during its passage through the cooling pipe.

The induction electromagnetic field was generated

NOMENCLATURE

At	Ampere–turn	R_i, R_e	inner and outer radii of the crucible
B	r.m.s. magnetic field	T	initial temperature of the bulk liquid
$\mathbf{B}_r, \mathbf{B}_z$	radial and axial components of **B**	T_f	melting point
c	specific heat	t	time
d	average diameter of the crystals	**u**	local velocity.
E	r.m.s. electric field		
$\bar{F}_z$	time mean vertical component of the electromagnetic body force	Greek symbols	
		α	thermal diffusivity
g	gravity	β	thermal expansion coefficient of liquid
Gr	Grashof number, $gR_e^3\beta\Delta T/\nu^2$	ΔT	superheat
H	liquid metal height	δ	electromagnetic skin depth
J	r.m.s. current density	η	viscosity
k	thermal conductivity	μ	magnetic permeability
L_f	latent heat of fusion	ν	kinematic viscosity
P	caloric power dissipated by Joule effect within the molten metal	ρ	density
		σ	electrical conductivity of liquid
Pr	Prandtl number, $\eta c/k$	ϕ	phase angle
r	radial position from the cooling pipe	ω	current angular frequency.

by an inductor made up of 140 jointed turns, distributed in five layers and traversed by an electric current of 50 Hz frequency. The coil height was 120 mm, the interior and exterior diameters being 250 and 290 mm, respectively. The magnetizing force was modulated at will, from 0 to 10 500 At, by an autotransformer.

3. MEASUREMENT TECHNIQUES

3.1. *Temperature measurement*

The temperatures were measured by means of a battery of six stainless-steel sheeted thermocouples 1-mm diam., spaced 1 cm apart and which could be aligned either horizontally along a radius, or vertically; in this latter case, it was possible to measure the temperatures in the near proximity of the hot wall. A six-channel recorder (Linseis No. 2000) enabled the evolution of the temperature field inside the melt during the solidification to be followed. The response time of this recorder permitted detection of the temperature fluctuations when their frequencies were less than 5 Hz.

The solidification tests were carried out according to the following procedure: beforehand, the melt was heated up to a temperature T_m, such as $T_m - T = 10°C$, T being the temperature corresponding to the superheat $\Delta T = T - T_f$, at which the experiment must be performed. When temperature T_m was reached, the electric current was turned off so that the liquid metal could cool slowly to the required superheat temperature T (under these conditions, experiments show that the bulk is practically isothermal, to within 2°C). The experiment was then started by delivering cooling water and continued until all the metal had solidified.

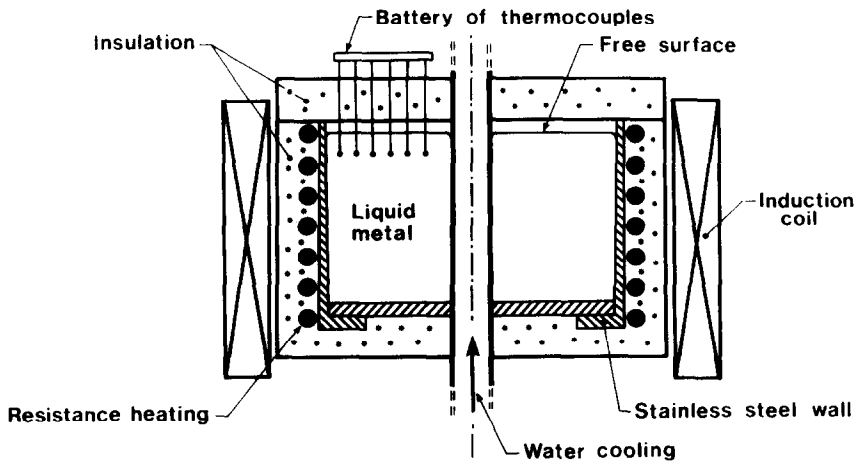

FIG. 1. Schematic diagram of the apparatus.

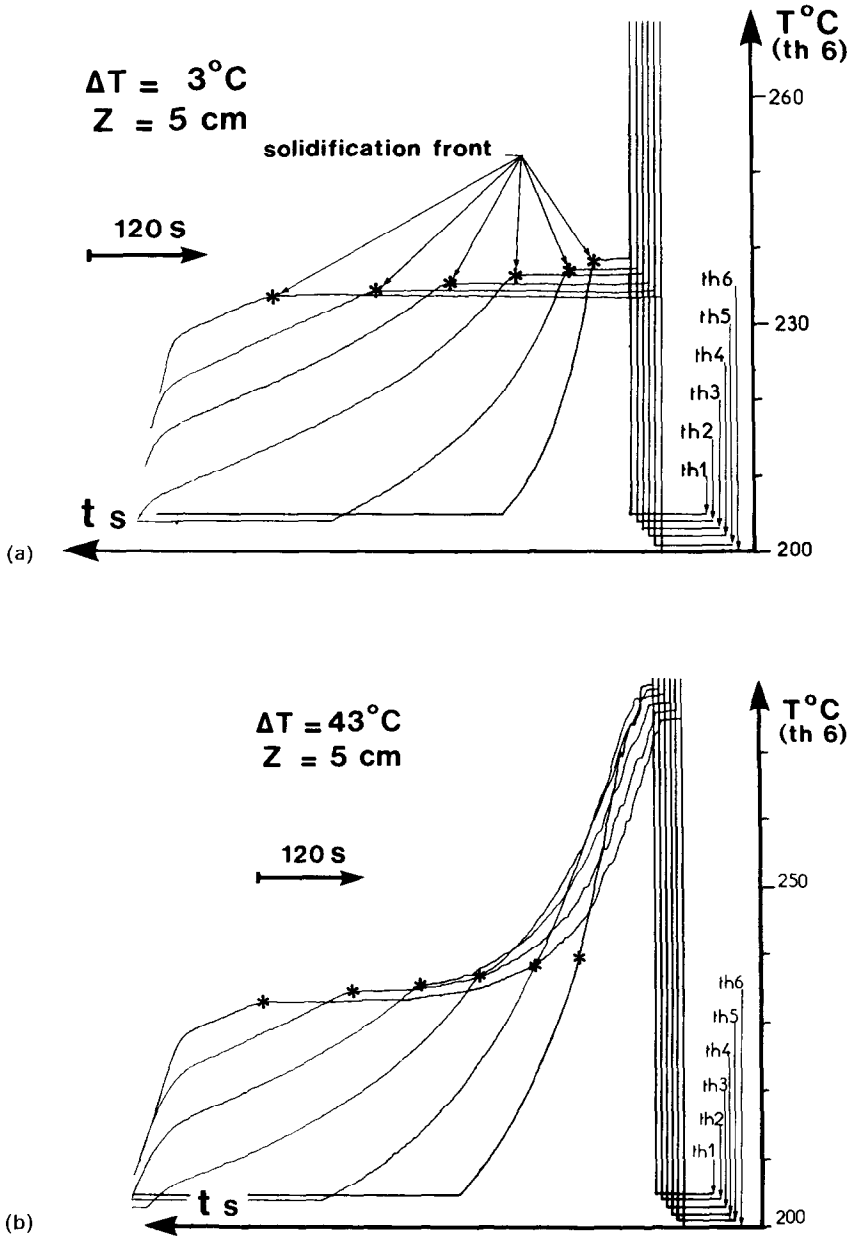

FIG. 2. Temperature fluctuations recorded at mid-height of the melt: (a) $\Delta T = 3°C$, (b) $\Delta T = 43°C$.

So as to avoid the superposition of the recordings, simultaneously given by the thermocouples, the five fountain pens were previously offset with respect both to the time and temperature origins. Thermocouple 6 (Fig. 2) corresponded to the origin of temperatures, the other pens were offset 1°C in turn; each pen was also successively displaced 5 s along the time axis.

3.2. *Velocity measurements*

Velocity measurements have been made with an incorporated magnetic probe, the working principle, the calibration technique and the behaviour at high temperatures of which have already been detailed in previous papers [7–9], to which we refer the reader. Consequently, we confine ourselves to summarizing its main properties: this sensor allows, by simple voltage measurements, the determination of the local and instantaneous values of the magnitude and direction of velocity, up to about 700°C.

3.3. *Electromagnetic parameter measurement*

The measurements of the current density **J** were founded on the application of Ohm's law, $\mathbf{J} = \sigma(\mathbf{E} + \mathbf{u} \times \mathbf{B})$ (where **J**, σ, **E**, **u** and **B** are the current density, the electric conductivity, the electric field, the velocity and the magnetic field, respectively) which reduces to $\mathbf{J} = \sigma\mathbf{E}$, because both the displacement currents and the product $\mathbf{u} \times \mathbf{B}$ are negligible. Hence,

the current density is proportional to the e.m.f. caused by the circulation of the electric field **E** along a current line; this voltage was obtained between the two electrode tips of a potential sensor.

The voltage which occurs at the end of a small coil, placed perpendicular to a time-varying magnetic field, is proportional to its r.m.s. **B**. In the case of an axisymmetric magnetic field, the coil yielded the vertical component $\mathbf{B}_z$ for a horizontal position and the radial component $\mathbf{B}_r$ for a position both vertical and perpendicular to a radius.

Finally, a phase meter (Bruël & Kjaer, type 2971) allowed measurement of the phase angle between the periodic parameters $\mathbf{B}_r$, $\mathbf{B}_z$ and **J**.

4. SOLIDIFICATION IN THE PRESENCE OF NATURAL CONVECTION

4.1. *Low initial superheat* ($\Delta T = 3°C$)

Experiments were performed with $T = 235°C$ whereas the melting point of the pure tin is 231.9°C. Figure 2(a) shows an example of recording carried out at the mid-height of the melt. The absence of temperature fluctuations may be seen; moreover, the sudden change of the slope of the recordings shows the moment when the solidification front comes into contact with the thermocouple tips, the locations of which were well known. Figure 3(a) presents the shape and position of the solid–liquid interface drawn for given times and reveals the unidimensional character of the heat transfer (the solidification front is practically vertical); the thermal gradients are in practice of zero value inside the bulk and it follows that the heat transfer is essentially conductive.

4.2. *High initial superheat* ($\Delta T = 43°C$)

The temperature of the bath was initially 275°C, in this case the caloric energy due to the superheat is of the order of 1/6 of the energy liberated by the latent heat of solidification $[L_f/C(T - T_f) \simeq 5.7]$.

Small fluctuations of temperature [Fig. 2(b)], observed during the early stages of cooling (i.e. in the presence of high superheat) reveal the occurrence of the natural convection. This effect is particularly marked for the thermocouple 1, which is located in the vicinity of the cold wall. Under the action of the buoyancy forces the fluid particles have a tendency to move upward along the hot wall and downward along the cold wall, but the velocity maps could not be plotted, because measurements showed that the peak velocities in the vicinity of the solidified crust were low, of the order of 2 cm s^{-1}.

At the initiation of freezing, the solidified crust is now inclined, because the heat transfer is no longer exclusively conductive [Fig. 3(b)]. Moreover, in the vicinity of the front, the thermal gradients decrease as the liquid–solid interface moves forward, i.e. as the superheat decreases; the superheat practically vanishes at half the time required for the complete solidification. When $t > 200$ s, the temperature of the bulk is very near

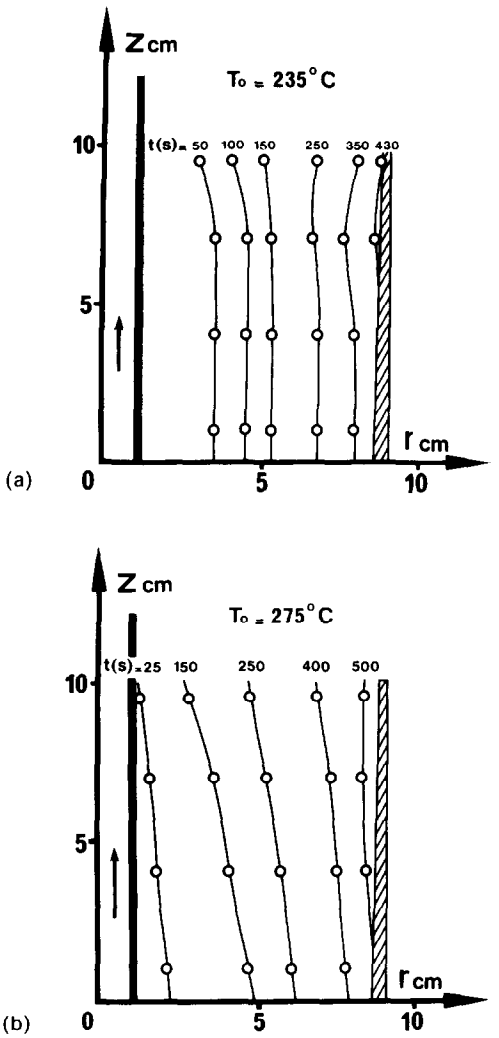

FIG. 3. Shape and position of the solid–liquid interface: (a) $\Delta T = 3°C$, (b) $\Delta T = 43°C$.

to the melting point. So, under these conditions, thermal transfers are again made by a purely conduction mode which results in a gradual re-establishment of a vertical front [Fig. 3(b)]. Moreover, at the early stages of freezing, the rate of movement of the solidification boundary is slightly slowed down, with respect to the case of Section 4.1.

Figure 4(a) presents map of isotherms, plotted for $t = 50$ s, which indicate the presence of a convective cell. This loop fills an upper zone corresponding to 3/4 of the volume occupied by the liquid metal. The fluid part situated in the lower zone of the melt seems mainly subjected to a conductive thermal transfer. The thermal gradients along the interface are much more pronounced in the upper part than in the neighbourhood of the bottom of the crucible; furthermore, the hotter zone (271°C) is located near the free surface. Figure 4(b) (plotted for $t = 110$ s) shows that the shape of the isotherms is not considerably modified; on the other hand, the averaged superheat drop is 27°C for 110 s.

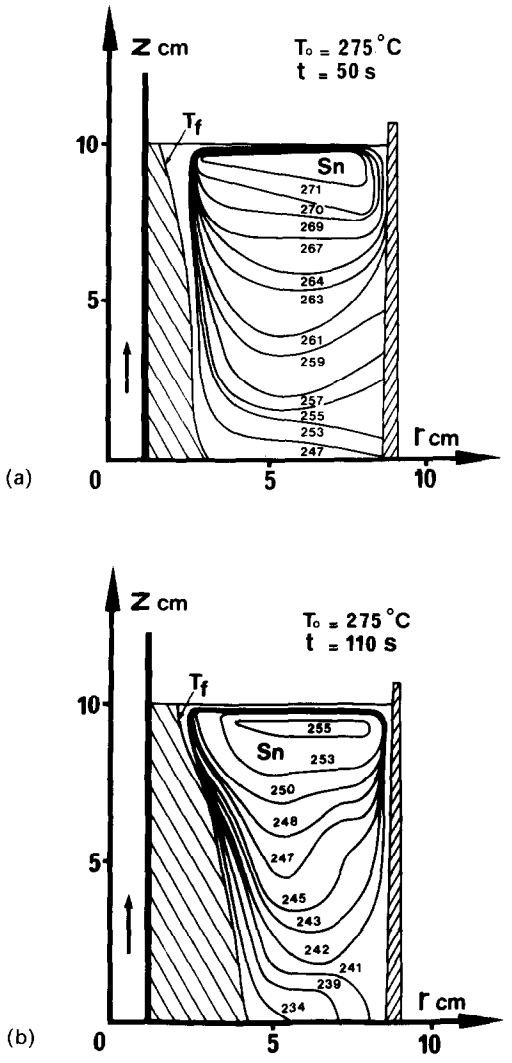

FIG. 4. Temperature fields in natural convection ($\Delta T = 43°C$): (a) $t = 50$ s, (b) $t = 110$ s.

5. SOLIDIFICATION IN THE PRESENCE OF FORCED CONVECTION (ELECTROMAGNETIC STIRRING)

When an alternating current circulates through a coil, an electromagnetic wave front diffuses into a crucible holding a liquid metal, ensuring that large eddy currents of current density **J** are induced in the metal. Moreover, for a metal of electric conductivity σ and magnetic permeability μ a 'skin effect' occurs, connected with a depth of penetration $\delta = (2/\sigma\mu\omega)^{1/2}$ of the magnetic field and electric current (i.e. **B** and **J** follow the $e^{-r/\delta}$ exponential law). Nevertheless, this relation is not rigorously exact both for the low frequencies and the crucibles of small radii.

The melt is subject to electromagnetic body forces due to the interaction of the induced current **J** and the axial and radial components of the magnetic field ($\mathbf{B}_r$ and $\mathbf{B}_z$). These Lorentz forces may be resolved into a potential part balanced by a pressure gradient, which results in the deformation of the free surface, and a rotational part, due only to the end effects and which is responsible for an electromagnetic stirring equivalent to a forced convection. The intensity of the forced convection depends on the magnitude of the magnetizing force, the frequency of the current, the geometries of the crucible and coil and, also, of the electromagnetic boundary conditions [10–15].

The creation of a forced convection by the electromagnetic stirring is an interesting technique because the rate of the liquid metal flow may be easily modulated at will, without contact with the melt, and hence without risk of pollution.

5.1. *Electromagnetic parameter measurements*

From methodical measurements of the current density inside a vertical and radial cross-section of the mold, we reach a caloric power dissipated by the Joule effect within the molten metal

$$P = \iiint_v \frac{J^2}{\sigma} dv = \frac{2\pi}{\sigma} \int_0^H \int_{R_i}^{R_e} J^2(r, z) r \, dr \, dz$$

where H, R_i and R_e are, respectively, the height of the bath and the interior and exterior radii of the annular mold.

We find that magnetizing forces of 4200 and 9800 Ampere–turns (At) correspond, respectively, to caloric powers of 67 and 365 W (i.e. in the latter case, 23% of the latent heat of solidification).

Methodical measurements of the r.m.s. of the current density **J** and of the radial component of the magnetic field $\mathbf{B}_r$, as well as the phase angle $\phi(\mathbf{J}, \mathbf{B}_r)$ allow determination of the time mean axial component of the electromagnetic body forces given by:

$$\bar{F}_z = J \cdot B_r \cos(\mathbf{J}, \mathbf{B}_r).$$

The vertical components $\bar{F}_z$ are primarily rotational [14] and so responsible for the stirring of the bath; consequently, knowledge of the $\bar{F}_z$ distribution will allow explanation of the fluid flow patterns.

It is difficult to carry out these measurements during a solidification, on account of the movement of the solidified crust. So, experimental runs using additional interior cylinders, of exterior radii R_i and fashioned from solid stainless steel, have been performed. These cylinders play the role of the solid phase to allow easier operation in the steady state. Distributions of $\bar{F}_z$ (Fig. 5) were plotted without water cooling, with a practically uniform temperature of 275°C, respectively, for $R_i = 1.2$ cm and $R_i = 4.85$ cm. It may be seen that, because of the electromagnetic skin depth, $\bar{F}_z$ decreases along a radius, from the outer wall towards the centre of the pool. The vertical forces are important within the half upper part of the crucible and insignificant inside the lower part; moreover, $\bar{F}_z$ is always directed downward, except for a small zone located in the vicinity of the vertical position defined by $z = 4$ cm.

The distribution of $\bar{F}_z$ is here different from that observed in the coreless induction furnace, where the

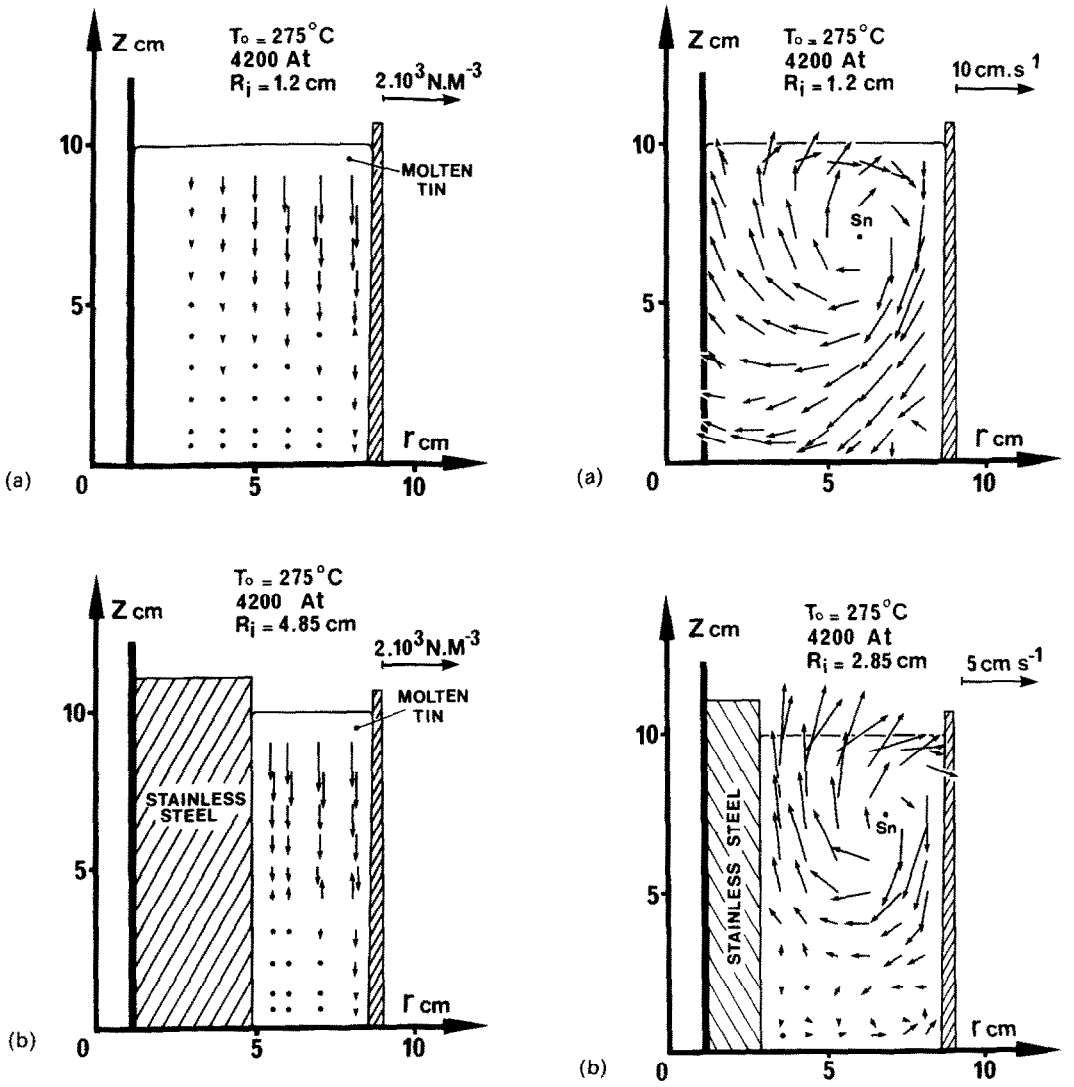

FIG. 5. Distribution of vertical component of the electromagnetic body forces: (a) $R_i = 1.2$ cm, (b) $R_i = 4.85$ cm.

vertical component of the electromagnetic forces are, approximately, symmetrically distributed with respect to the horizontal plane of symmetry of the crucible. In our furnace, the horizontal lower wall and especially the crown, mentioned in Section 2 and shown in Fig. 1, are conducting and behave as an electromagnetic screen [15]. The eddy currents, which circulate through the shield, are practically opposite in phase to those of the inductor; this results in additional body forces arising that are opposite to the rotational forces created by the coil. Consequently, the resultant electromagnetic force field is considerably attenuated in the lower part of the mold.

5.2. *Velocity measurements*

The velocity maps, presented in Fig. 6, were plotted without cooling, in order to avoid the solidification of the bath. The progression of the front, which results in a modification in time of the geometry of the annular

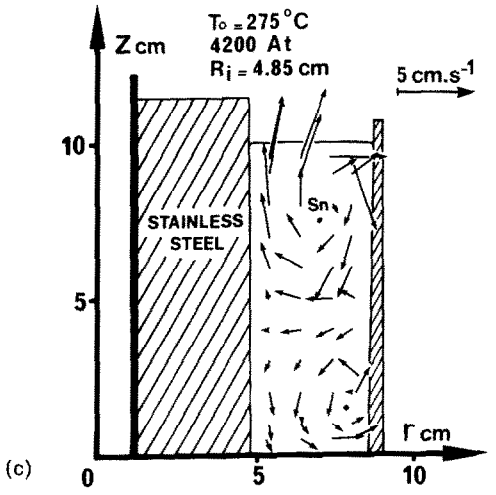

FIG. 6. Measured velocity fields in forced convection: (a) $R_i = 1.2$ cm, (b) $R_i = 2.85$ cm, (c) $R_i = 4.85$ cm.

pool and of the boundary conditions, has again been simulated by the adjunction of two cylinders made of solid stainless steel, the exterior radii R_i of which were 2.85 and 4.85 cm, respectively.

Inspection of Fig. 6(a) (connected with the start of the solidification, i.e. $R_i = 1.2$ cm) reveals the presence of a single loop; on the other hand, for an excitation of 4200 At, the vertical components of the velocity are of the order of 5 and 10 cm s^{-1}, in the vicinity of the walls of the inner and outer cylinders, respectively. It may be seen, in Fig. 6(b) ($R_i = 2.85$ cm) that the velocities decrease, especially inside the lower part of the mould, where a new recirculating vortex occurs, but a vortex in which the fluid flows the opposite way relative to the upper one. In the case depicted in Fig. 6(c) ($R_i = 4.85$ cm), the volume of the upper cell decreases in favour of the lower loop; however, the volume of the lower vortex remains the weaker. The velocities along the wall representing the solid–liquid interface are about twice as large inside the upper cell than in the lower recirculating loop.

Finally, complementary experiments establish that the velocity vectors are proportional to the magnetizing force.

In summary, inside the melt and particularly near the wall, the velocities decrease as the solidified crust advances. Moreover, the initial single cell is replaced by two contra-rotating vortices which are similar, only from the point of view of the aspect, with the typical fluid flows within a coreless induction furnace. This flow structure can be easily understood by examination of the $\bar{F}_z$ maps (Fig. 5); apparently the upper loop is principally driven by the vertical component of the electromagnetic body forces, whereas the lower cell seems to be mainly induced by the upper one (viscous effect).

5.3. *Temperature fluctuations*

The recordings depicted in Fig. 7(a) were obtained for a magnetizing force of 2100 At and $Z = 5$ cm. In the zone occupied by the liquid phase may be seen a superposition of recordings showing that the stirring is still unable to homogenize the temperature in the core of the melt. At the start of the circulation of the cooling water, strong temperature fluctuations, liable to reach 14°C, occur; this effect is quite marked for the recording given by the thermocouple 1, which is the nearest to the cooling pipe. This event is provoked by dragging of the fluid elements caused by the electromagnetic stirring [Fig. 6(a)]; at the initiation of the stirring, a steep thermal gradient exists between the two cylindrical walls and the fluid particles, carried away by the vortex, travel alternately from a hot to a cold fluid zone. At this stage, the random oscillations of temperature indicate that the convection movements are not yet well established in the molten tin. Furthermore, the turbulence intensity is not high enough to promote rapid transfer through the fluid layers.

On the contrary, the recordings presented in Figs. 7(b) and (c), dealing with an increasing of the magnetizing force, show that the tendency to a superposition of the recordings is markedly subdued for 4200 At and virtually removed for 6400 At. The stirring is adequate now and the intensity of turbulence is sufficient to homogenize the temperature inside the bulk. The effects also result in a pronounced damping to the temperature oscillations, which become less than 1°C, for an excitation of 6400 At.

5.4. *Shape and movement of the melt–solid interface*

Figure 8 shows that, after $t = 100$ s, the solidification front exhibits two zones of concave shape, the locations of which coincide with those of the recirculating loops, pointed out in Figs. 6(b) and (c); from $t = 250$ s, the solidification front becomes gradually vertical because both the stirring intensity and the superheat are markedly attenuated.

Figure 9 presents the evolution with time of the solid metal thickness. Inside the experimental range the degree of stirring does not have a marked impact on the rate of movement of the interface. Moreover, comparisons with experiments performed in the case of natural convection, for the same initial superheat, show a slight decrease of the rate of movement of the front, within the first half of the time required for complete solidification. For a given interface position, the superheat decreases as the intensity of stirring increases. Experiments show that, for a magnetizing force of 4200 At, the superheat virtually vanishes after one third of the time necessary for the whole phase change.

Figure 10 shows a sketch depicting the dependence of the superheat on the radius r of the solidified crust (measured for $z = 5$ cm). Its inspection confirms the primary effect of the forced convection on the withdrawal of heat within the core of the melt.

Temperature fields, plotted for $t = 50$ s and $t = 110$ s, are sketched in Fig. 11. Examination of Fig. 11(a) yields support to the presence of the two vortices, already revealed by means of velocity measurements; it may be seen that, in the bulk liquid, the temperature is uniform to within 4°C. Furthermore, the hotter zone is located in the near vicinity of the eye of the lower loop, while in the case of natural convection, for an identical superheat and the same duration of solidification ($t = 50$ s), the hot zone was situated near the free surface of the melt [Fig. 4(a)]; in this last instance, the difference between the extreme temperatures (i.e. from top to bottom) was 24°C. Figure 11(b) shows again that forced convection leads to rapid dissipation of superheat (34°C in 110 s); moreover, it may be seen that the bulk liquid is now almost isothermal to within 1°C.

6. METALLOGRAPHIC STUDY AND DISCUSSION

Macroetching methods have been used, in order to reveal the macrostructure of samples cut from commercially pure tin ingots. A comparative metallographic study has been made on samples correspond-

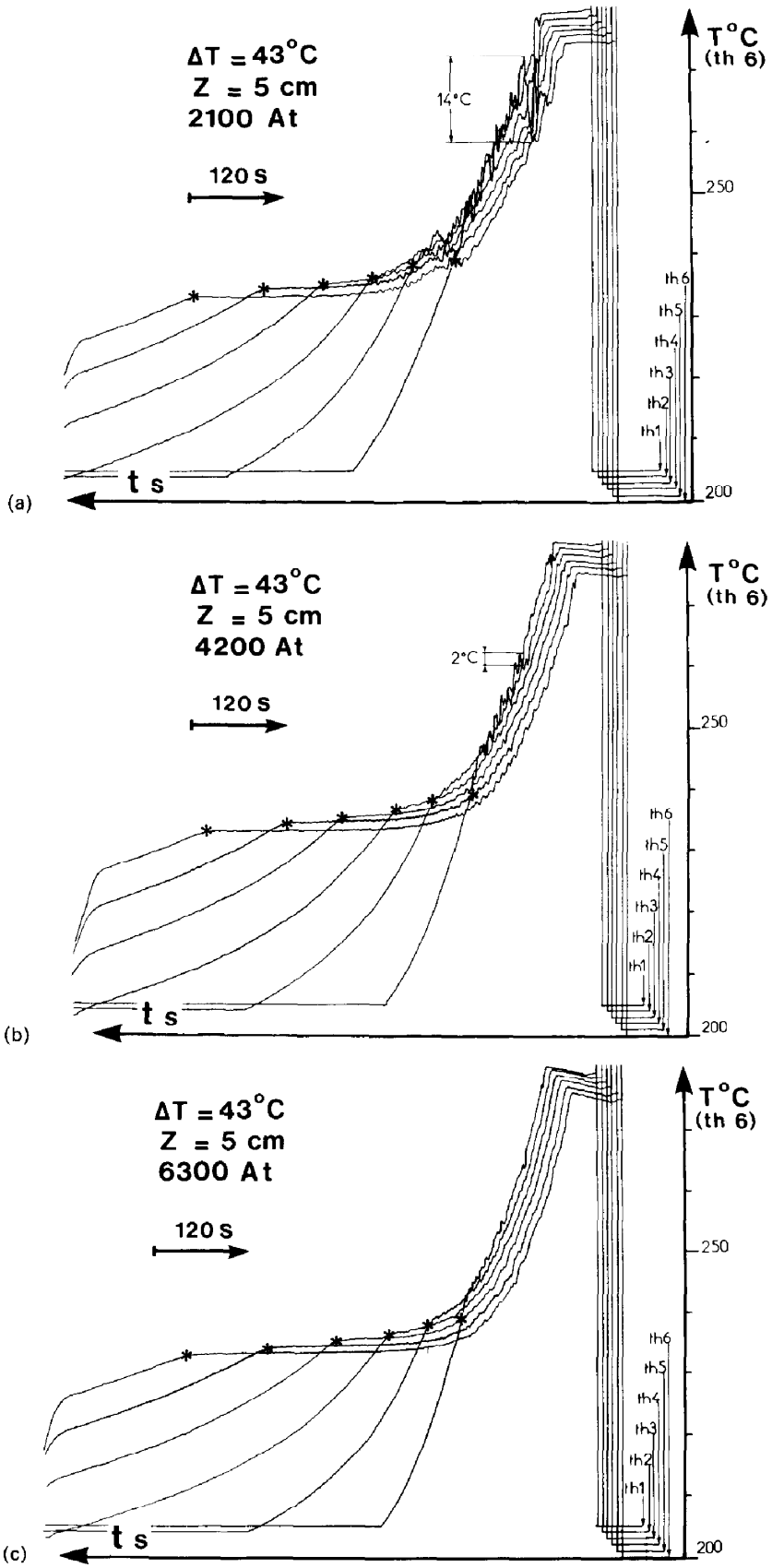

FIG. 7. Temperature fluctuations recorded at mid-height of the melt ($\Delta T = 43°C$): (a) 2100 At, (b) 4200 At, (c) 6300 At.

Table 1. Thermophysical properties of tin

			232°C ($\Delta T = 0$)	275°C ($\Delta T = 43$°C)	332°C ($\Delta T = 100$°C)
ρ	density	$kg\ m^{-3}$	6.98×10^3	6.95×10^3	6.91×10^3
η	viscosity	$kg\ m^{-1}\ s^{-1}$	1.97×10^{-3}	1.78×10^{-3}	1.57×10^{-3}
ν	kinematic viscosity	$m^2\ s^{-1}$	2.82×10^{-7}	2.56×10^{-7}	2.27×10^{-7}
α	thermal diffusivity	$m^2\ s^{-1}$	315.00×10^{-7}	294.00×10^{-7}	197.00×10^{-7}
σ	electrical conductivity	$\Omega^{-1}\ m^{-1}$	2.13×10^6	2.09×10^6	2.04×10^6
c	specific heat	$J\ kg^{-1}\ K^{-1}$	2.77×10^2	2.49×10^2	2.45×10^2
k	thermal conductivity	$J\ s^{-1}\ m^{-1}\ K^{-1}$	61.03	51.00	33.44
L_f	latent heat of fusion	$kJ\ kg^{-1}$	60.70×10^{12}		
Pr	Prandtl number		0.0089	0.0087	0.0115
Gr	Grashof number		0	6.51×10^8	19.25×10^8

ing to the absence and presence of various intensities of stirring and different degrees of superheat. Slices, of about 15-mm thick and 100-mm height, were cut along whole radial and vertical cross-sections of the annular ingots. For each macrography presented here, the left-hand side is connected with the cooling pipe and the right-hand side with the outer wall of the crucible.

6.1. *Natural convection*

Figure 12 shows that the inclination of the columnar crystals increases as the superheat increases. When the superheat is very low [$\Delta T = 3$°C, for the case of Fig. 12(a)], the crystals grow horizontally; in agreement with the remark expressed after inspection of Fig. 3(a), this effect is due to the absence of convection, which results in a purely conductive and radial heat transfer.

The presence of an angle of inclination (defined with respect to the horizontal) is indicated in Figs. 12(b) and (c), corresponding to 43 and 100°C of superheat, respectively. The columnar zone is more and more inclined in the upstream direction, because the thermal convection is progressively enhanced inside a single cell, where the fluid flows upward along the hot wall and downward along the cooling pipe; this phenomenon has been particularly studied by Takahashi and Ichikawa [17] who have demonstrated that the inclination of the dendrites was provoked by an imbalance of the solute content between upstream and downstream sides of the columnar tips, which behave as obstacles; the solute would be rejected from the upstream side and accumulated downstream. This explanation may not be reliable for the case of a commercially pure metal; however, it has been proved [17] that very small quantities of alloying elements are sufficient to produce a notable inclination of the dendrites of a commercially pure aluminium.

Furthermore, the enhancement of the natural convection results in a slight decreasing of the average diameter d of the crystals. This effect is passably pronounced at the early stages of freezing, and then vanishes, approximately at mid-radius, on account of the evacuation of superheat (already mentioned), obviously followed by a quite marked damping of the free convection.

6.2. *Electromagnetic stirring*

The macrostructures presented in Fig. 13 have been yielded from the same excitation (4200 At) and various degrees of superheat. At the onset of freezing (corresponding to a thickness of the solidifying ingot of

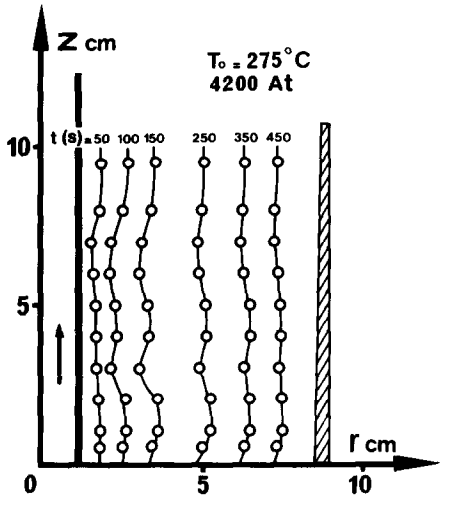

FIG. 8. Shape and position of solid–liquid interface (4200 At and $\Delta T = 43$°C).

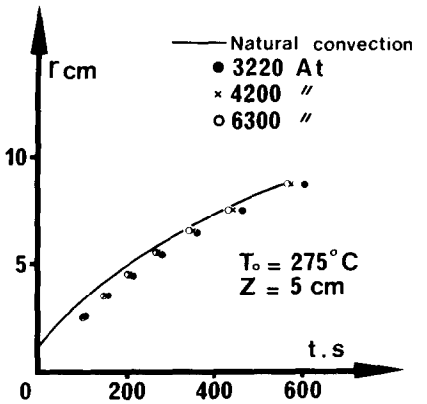

FIG. 9. Thickness of solid metal during solidification in natural convection and for various stirring intensities.

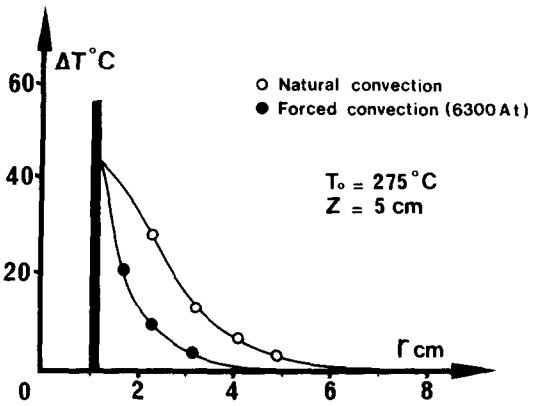

FIG. 10. Superheat drop as a function of the thickness of the solidified crust, in natural and forced convection.

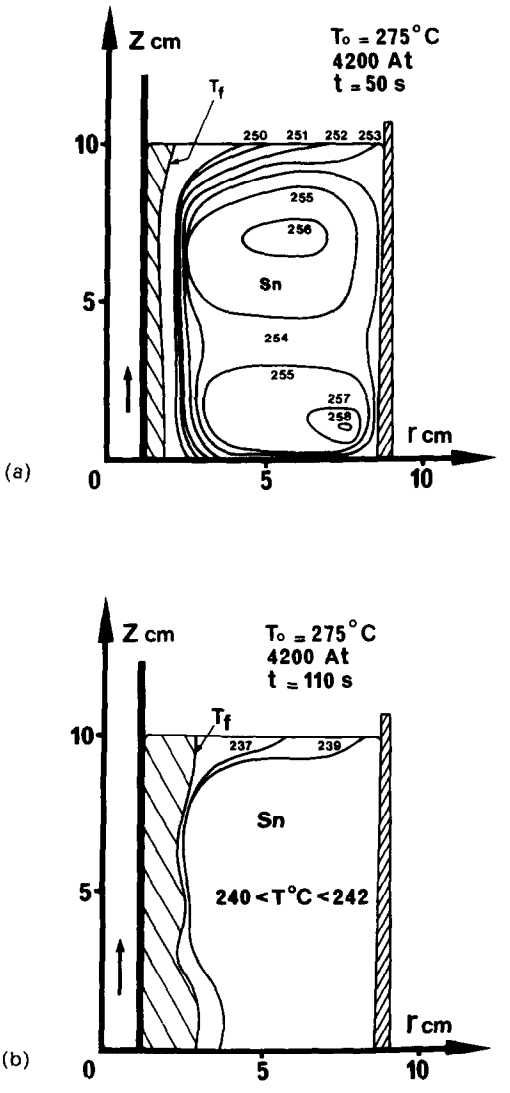

FIG. 11. Temperature fields in forced convection: (a) $t = 50$ s, (b) $t = 110$ s.

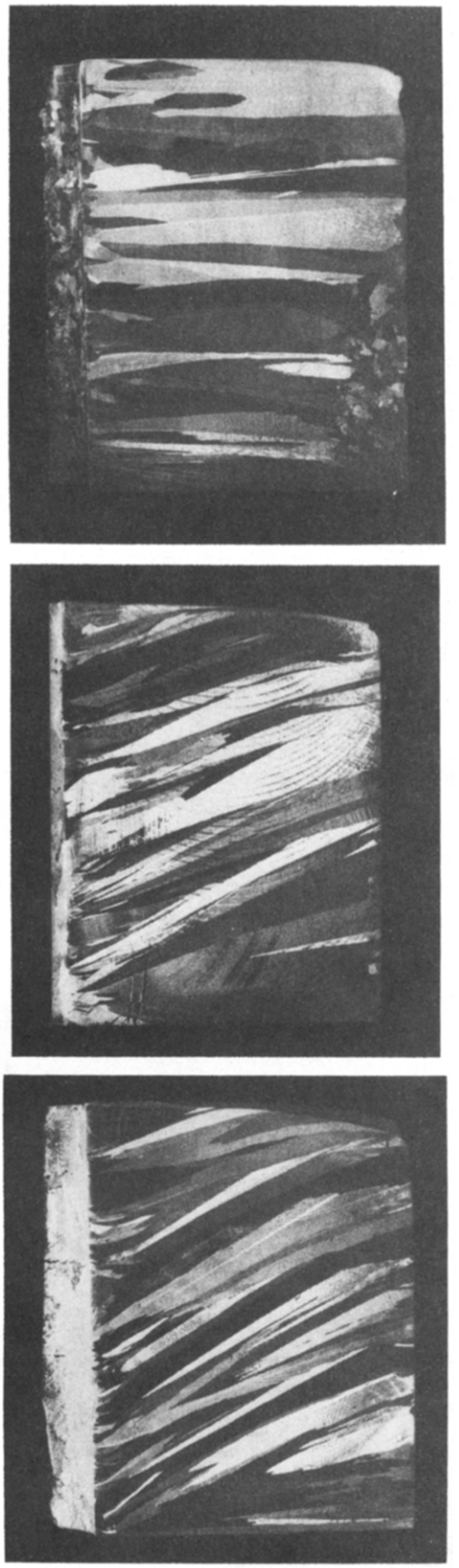

FIG. 12. Macrostructures of commercially pure tin, solidified in natural convection and from various superheats: (a) $\Delta T = 3°C$, (b) $\Delta T = 43°C$, (c) $\Delta T = 100°C$.

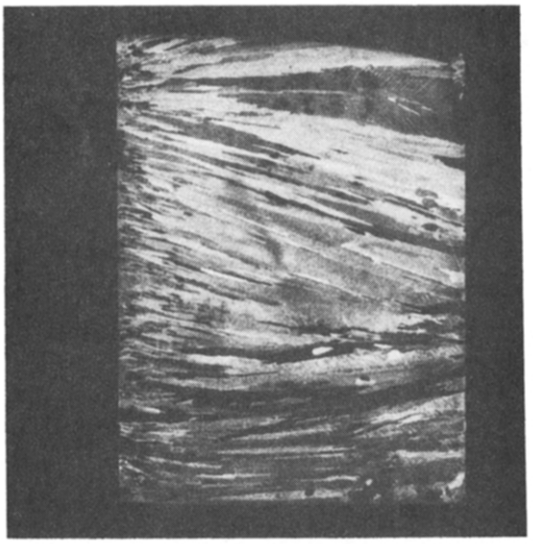

(a)

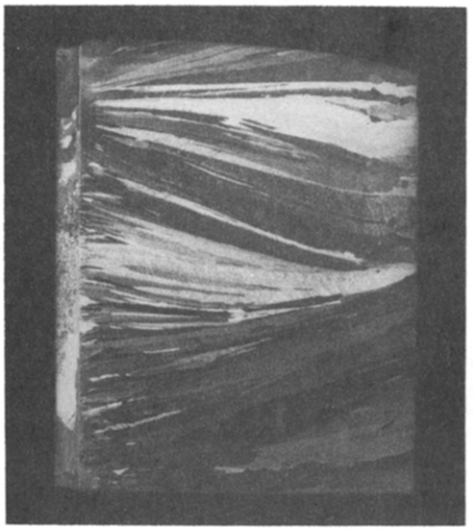

(b)

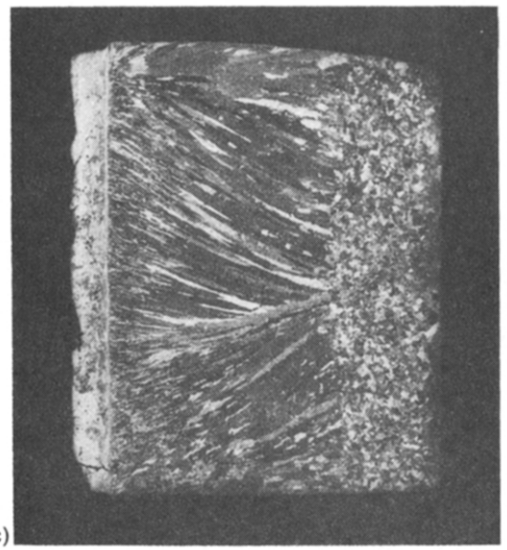

(c)

FIG. 13. Macrostructures of commercially pure tin, solidified from a magnetizing force of 4200 At and various degrees of superheat: (a) $\Delta T = 3°C$, (b) $\Delta T = 43°C$, (c) $\Delta T = 100°C$.

the order of 1 cm), the dendrites are almost all inclined in the same direction (i.e. downward); this observation may be explained by the effect of the single cell depicted in Fig. 6(a). When the thickness of the solid phase passes beyond 2 cm it may be seen that the columns are inclined downward in the upper part of the solidifying ingot and upward in the lower part. The height of these zones may be easily connected with the size and the direction of circulation of the two vortices seen in Figs. 6(b) and (c).

The effect of the superheat consists in a decreasing of the average diameter of the crystals and in an increasing of their inclination; it must be noted that the viscosity of the molten tin decreases by about 30% when the temperature rises from 235 to 332°C. On account of the impact of the superheat on the inclination of the dendrites (Fig. 13), the measurement of the inclination α is only a very crude method to estimate the flow rate in the vicinity of a solid–liquid interface. Finally, an equiaxed structure occurs, within a peripheral zone of 3-cm thick, for a superheat of 100°C [Fig. 13(c)].

Figure 14 shows two samples obtained from a magnetizing force of 9940 At and superheats of 3 and 43°C. By comparison of Figs. 13 and 14, it appears that the augmentation of the stirring intensity, for the same superheat, results in a decreasing of the average diameter d of the columns and in an enhancement of their inclination. On the other hand, a coarse equiaxed structure, located within a cortical area, of about 2-cm thick, may again be observed.

Comparison between Figs. 12(b) and 14(b) shows that, on average, d is divided by 5 and the number of crystals multiplied by 25, when the magnetizing force rises from 0 to about 10 000 At.

7. CONCLUSIONS

As a first step, the electromagnetic force pattern has been obtained from electromagnetic parameter measurements (current density **J**, radial and axial components, $\mathbf{B}_r$ and $\mathbf{B}_z$, of the magnetic field and phase angle between these periodic parameters).

Velocity measurements have been made in the molten tin bath using a newly developed magnetic probe. Through the use of this sensor a simple voltage measurement allows the determination of the local instantaneous values of the velocity vector at temperatures up to about 700°C. By this means maps were obtained of the velocity fields, for various stirring intensities and various positions of the solidification front. The understanding of the evolution of the velocity field has been given by inspection of the electromagnetic force distribution.

The velocity measurements were augmented by temperature measurements. These temperature data allowed us to follow the evolution of the solidification front and of the superheat with time. Experiments were carried out for various degrees of superheat, both in the absence and presence of electromagnetic stirring, which allowed the assessment of the role played by thermal

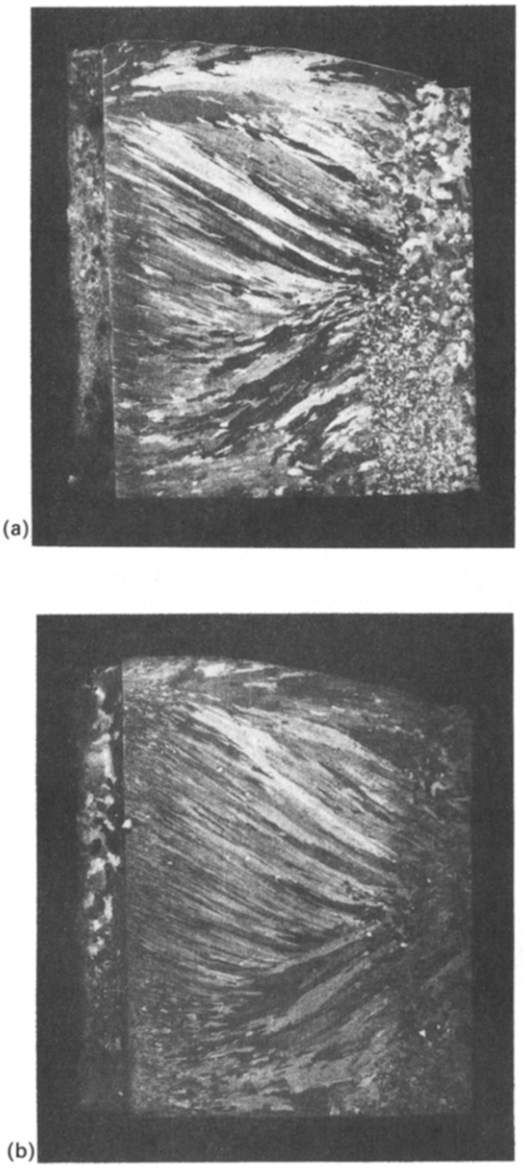

FIG. 14. Macrostructures of commercially pure tin, solidified from a magnetizing force of 9940 At and various degrees of superheat: (a) $\Delta T = 3°C$, (b) $\Delta T = 43°C$.

natural convection. The forced convection was found to promote both evacuation of superheat and rapid homogenization of the bulk liquid.

Finally, the macrostructure of the solidified melt was also examined and the metallurgical findings connected with the heat and fluid flow measurements. To summarize, this experimental work reveals the primary hydrodynamic effects on the thermal and metallurgical phenomena; particularly, the crystals growing are in agreement with the evolution of the metal flow patterns.

REFERENCES

1. H. S. Marr, Electromagnetic stirring: stepping stone to improved continuously cast products, *Iron Steel Int.* **2,** 29–41 (1979).
2. D. B. Spalding and N. H. Afgan, *Heat and Mass Transfer in Metallurgical Systems.* McGraw-Hill, New York (1981).
3. A. A. Tsavaras and H. D. Brody, Electromagnetic stirring and continuous casting—achievements, problems and goals, *J. Met.* **1,** 31–37 (1984).
4. J. Szekely and P. S. Chhabra, The effect of natural convection on the shape and movement of the melt–solid interface in the controlled solidification of lead, *Met. Trans.* **1,** 1195–1203 (1970).
5. A. W. Hills, S. L. Malhotra and M. R. Moore, The solidification of pure metals (and eutectics) under unidirectional heat flow conditions: II. Solidification in the presence of superheat, *Met. Trans. B* **6,** 131–142 (1975).
6. C. Gau and R. Viskanta, Melting solidification of a metal system in a rectangular cavity, *Int. J. Heat Mass Transfer* **27,** 113–123 (1984).
7. R. Ricou and Ch. Vives, Local velocity and mass transfer measurements in molten metals using an incorporated magnet probe, *Int. J. Heat Mass Transfer* **25,** 1579–1588 (1982).
8. J. L. Meyer, F. Durand, R. Ricou and Ch. Vives, Steady flow of liquid aluminum in a rectangular-vertical ingot mold, thermally or electromagnetically activated, *Met. Trans. B* **3,** 471–478 (1984).
9. H. C. Lee, J. W. Evans and Ch. Vives, Velocity measurement in Wood's metal using an incorporated magnet probe, *Met. Trans. B* **4,** 734–736 (1984).
10. E. Tarapore and J. W. Evans, Fluid velocities in induction melting furnaces: Part I. Theory and laboratory experiments, *Met. Trans. B* **7,** 343–351 (1976).
11. E. Tarapore, J. W. Evans and J. Langfeldt, Fluid velocities in induction melting furnaces: Part II. Large scale measurements and predictions, *Met. Trans. B* **8,** 179–184 (1977).
12. J. Szekely, C. Chang and R. Ryan, The measurement and prediction of the melt velocities in a turbulent electromagnetically driven recirculating low melting alloy system, *Met. Trans. B* **8,** 333–338 (1977).
13. N. El-Kaddah and J. Szekely, The turbulent recirculating flow field in a coreless induction furnace, a comparison of theoretical predictions with measurements, *J. Fluid Mech.* **133,** 37–46 (1983).
14. D. Moore and J. Hunt, *Liquid Metal Flows and Magnetohydrodynamics*, pp. 359–373. A.I.A.A., New York (1983).
15. Ch. Vives and R. Ricou, Fluid flow phenomena in a single phase coreless induction furnace, *Met. Trans. B*, in press.
16. T. Takahashi, K. Ichikawa and M. Kudou, *Solidification and Casting of Metals*, pp. 331–342. Metals Society, Sheffield (1977).

EFFETS D'UN BRASSAGE ELECTROMAGNETIQUE DURANT LA SOLIDIFICATION CONTROLEE DE L'ETAIN

Résumé—On étudie le rôle des convections naturelle et forcée durant la solidification contrôlée de l'étain pur dans un creuset annulaire. La convection forcée est produite par brassage électromagnétique. Des cartes du champ de force électromagnétique et du champ de vitesse ont été obtenues pour différentes intensités de brassage et différentes positions du front de solidification. Des mesures thermiques ont permis de suivre l'évolution du front de solidification dans le temps. Ces expériences ont été conduites pour différentes valeurs de la surchauffe, en absence et en présence de brassage électromagnétique. Une discussion, reliant les résultats métallurgiques (macrostructure) aux mesures thermiques et hydrodynamiques, est présentée.

EINFLUSS EINER ELEKTROMAGNETISCH BEWIRKTEN KONVEKTIONSSTRÖMUNG AUF DIE ERSTARRUNG VON ZINN

Zusammenfassung—Es wurde der Einfluß der natürlichen und erzwungenen Konvektion während der Erstarrung von reinem Zinn in einem ringförmigen Behältnis untersucht. Die erzwungene Konvektion wurde elektromagnetisch bewirkt. Elektromagnetische Feldstärke und Geschwindigkeitsfeld wurden für verschiedene Bewegungsintensitäten und verschiedene Lagen der Erstarrungsfront ermittelt. Temperaturmessungen ermöglichten es, das Fortschreiten der Erstarrungsfront in Abhängigkeit von der Zeit zu verfolgen. Diese Experimente wurden für verschiedene Überhitzungsgrade sowohl mit als auch ohne elektromagnetische Anregung durchgeführt. Die metallurgischen Erkenntnisse (Makrostruktur) werden anhand der Messungen von Wärme- und Flüssigkeitsstrom diskutiert.

ЭФФЕКТЫ ЭЛЕКТРОМАГНИТНОГО ПЕРЕМЕШИВАНИЯ В КОНТРОЛИРУЕМОМ ПРОЦЕССЕ ОТВЕРДЕВАНИЯ ОЛОВА ПРИ ЭЛЕКТРОМАГНИТНОМ ВОЗДЕЙСТВИИ

Аннотация—Изучается роль естественной и вынужденной конвекций при отвердевании чистого олова в кольцевом тигеле. Вынужденная конвекция была вызвана воздействием электромагнитного поля. Получены распределения электромагнитных сил и полей скорости для различных интенсивностей перемешивания и положений фронта отвердевания. Измерения температуры позволили проследить эволюцию во времени фронта отвердевания. Эксперименты проводились при разных уровнях перегрева как в отсутствие, так и при наличии электромагнитного поля. Обсуждается связь между макроструктурами и измеренными значениями потоков массы и тепла в жидкости.